ACS OMEGA

http://pubs.acs.org/journal/acsodf

Article

Investigation on the Thermo-Oxidative Degradation of Polyethylene, Poly(vinyl chloride), and Polystyrene Using $NiPIm_{1.5}$ and $NiPIm_2$ Nanocomposites

Rudrarapu Aravind,* Akash Kumar Sahu, Gouri Sankhar Brahma, and Trilochan Swain

Cite This: *ACS Omega* 2021, 6, 29869−29881

Read Online

ACCESS | Metrics & More | Article Recommendations | Supporting Information

ABSTRACT: In this work, we report the synthesis of two nanoscale composites of nickel, $NiPIm_{1.5}$ and $NiPIm_2$ ($NiPIm_{1.5}$ = $[Ni(C_3H_4N_2)(H_2O)_5](HPO_4)\cdot(H_2O)\cdot 0.3(C_3H_4N_2)$ and $NiPIm_2$ = $[Ni(C_3H_4N_2)(H_2O)_5](HPO_4)(H_2O)\cdot 0.4(C_3H_4N_2)\cdot H_2O$), characterization by various instrumental methods and the investigation of the thermo-oxidative degradation of polyethylene (PE), poly(vinyl chloride) (PVC), and polystyrene (PS) in the presence of both nanocomposites. All of these polymers are subjected to thermal treatment with and without composites at 353 K for 120 min. The rate of degradation is maximum with $NiPIm_2$ for all three polymers, PE—13.1522%, PS—13.6152%, and PVC—8.04%, whereas with $NiPIm_{1.5}$, PE—7.3128%, PS—11.9837%, and PVC—4.9106%. The percentage of degradation in the presence of composites is much greater than the percentage of degradation without composites. The specific heat capacities of $NiPIm_{1.5}$ and $NiPIm_2$ are −148.42 and −348.64 J kg^{-1} K^{-1}, respectively. The degradation process takes place by free radical mechanism. Thermogravimetric and differential thermal analyses revealed that the temperatures corresponding to the formation of composite materials with $NiPIm_2$ are 338.76, 331.78, and 354.30 K for PE, PVC, and PS, respectively. The temperatures of formation of the above composites are found to be less than that of $NiPIm_{1.5}$. The degraded residues of polymers indicate that ester is formed in each case along with other byproducts containing imidazole. Infrared studies revealed the thermal oxidation of hydroperoxides and the formation of ketone.

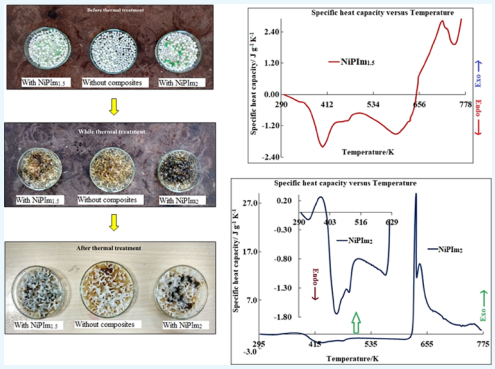

1. INTRODUCTION

The use of nonbiodegradable materials containing polyethylene, poly(vinyl chloride), and polystyrene is increasing day by day due to their high degree of consumer adaptability and low price. Consequently, the global production and use of synthetic polymers and plastic materials are rapidly escalating.[1] Post use, these materials get accumulated as pollutants, posing a potential threat to the environment. These pollutants have drastically affected both fresh water and marine water ecosystems, though of late, their use has been restricted to a certain extent by some of the countries. Due to the enormous volume of plastic waste and environmental concerns, plastics recycling has become a central theme in the modern plastics sector. The design of environmentally acceptable, cost-effective methods to reduce plastic waste is challenging due to the extreme complexity inherent in polymer recycling.

Degradation of polymers can be achieved by many techniques such as thermal,[2] thermo-oxidative,[3] photo-oxidative,[4] or by chemical exposure of materials using hydrolysis,[5] ultrasonic,[6] and plasma treatment.[7] Some of these degradation techniques, their experimental details, and outcomes are tabulated in Tables S1−S3. Degradation is frequently due to changes in the chemical and/or physical structure of the polymer chain, resulting in a reduction in the polymer's molecular weight. These changes might be unwanted, such as modifications during usage, or desired, such as biodegradation or the intentional reduction of a polymer's molecular weight. The influence of these variables on the molecular structure of the polymer is largely responsible for these alterations. It relies on its structure and the susceptibility to degradation of a polymer. Aromatic epoxies and chains are particularly vulnerable to ultraviolet breakdown, whereas thermal-sensitive hydrocarbon-based polymers typically are not appropriate in high-temperature applications.[8]

Researchers and engineers around the globe are on quest toward metal-assisted thermal degradation of such materials. Jen-hou and Schwartz carried out some experiments to degrade the polyethylene using some bacteria.[9] Nisar et al.[10] studied the thermal decomposition of poly(vinyl chloride) (PVC) in the presence of catalysts of commercially available oxides in the temperature range of 473−923 K. Kaplan et al. studied the

Received: August 12, 2021
Accepted: October 4, 2021
Published: October 28, 2021

biodegradation of polystyrene using 17 species of fungi, but the decomposition rate is very low, even on the addition of cellulose and minerals.[11] Zhu used ammonium polyphosphate to degrade polystyrenes under various conditions. He found that this polyphosphate accelerated the thermal degradation of polystyrene in N_2 atmosphere due to its acidity.[12] Among the biodegradable polymers, polyester amides (PEAs) play a pivotal role because of their high thermal stability and mechanical properties.[13] These are applied for the manufacture of a wide range of materials, such as disposable bags, matrix resins used as biomedical materials and drug carriers, etc.

In this context, we made an attempt to degrade the polymers (PE, PVC, and PS) using nickel imidazole nanocomposites, $NiPIm_{1.5}$ and $NiPIm_2$. These materials are well characterized. For degradation experiments, PE food packing stick covers, commercially available PVC grains, and PS food serving bowls were considered. Partial thermo-degradation of the above-mentioned polymers has been achieved, and the degradation mechanism has been established by means of infrared, thermogravimetric, and differential thermal analyses. To the best of our knowledge, no degradation studies were reported using a nickel imidazole composite at 353 K. The thermal properties of composites have been determined by the calorimetric study. The degradation process has been accelerated by both materials ($NiPIm_{1.5}$ < $NiPIm_2$) due to their heat dissipation property determined by the DSC analysis.

2. RESULTS

2.1. FTIR Analysis. Assignment of IR bands in the range 400−4000 cm^{-1} for both composites $NiPIm_{1.5}$ and $NiPIm_2$ is tabulated in Table 1.

Table 1. IR Data of $NiPIm_{1.5}$ and $NiPIm_2$

sl. no.	$NiPIm_{1.5}$	$NiPIm_2$	assignment
1	438.36	449.32	ν(Ni−N)
2	509.59, 570.68	515.07, 569.32	bending mode of P−O
3	626.31	621.98	N−H bend out of plane
4	663.01	661.87	torsion vibration
5	761.83	763.34	C−H bend out of plane
6	835.44	829.04	ν_{as}(P−O−P) bridge
7	901.21	896.98	ring bend of imidazole
8	1049.72	1051.81	C−H bend
9	1101.37	1101.37	$\nu_s(PO_3)^{2-}$ end group
10	1178.08	1180	ν(C−N) imidazole
11	1320.55	1318.21	C−H bend
12	1437.77	1433.99	ring stretch + N−H bend
13	1584.39	1586.07	ring stretch (νC═N)
14	1638.36	1660.27	O−H, H_2O vibrations
15	2982.87, 3144.96	2977.44, 3140.71	C−H stretching
16	3384.47	3413.70	O−H + N−H stretching

The bands at 438 and 449 cm^{-1} are assigned to the stretching vibrations of Ni−N for both composites.[18] The bands ascribed to the bending mode of P−O are in good accordance with the published literature by Rudrarapu and Aravind.[17,19] The stretching vibration of C ═ N is shifted from 1675 to 1584 cm^{-1} in $NiPIm_{1.5}$ and to 1586 cm^{-1} in $NiPIm_2$. The stretching frequency of C−N is shifted from 1250 to 1178 cm^{-1} in $NiPIm_{1.5}$ and to 1180 cm^{-1} in $NiPIm_2$. Both the stretching frequencies appear as a broad shoulder at a frequency of 1101 cm^{-1}. These bands are assigned according to the literature.[20] This indicates that in both the materials, the metal nickel is bonded with the pyridine-N atom of the imidazole ring rather than the pyrrole-NH atom. Due to the intermolecular hydrogen bonding with HPO_4 ion, the N−H stretching vibration of imidazole is shifted to 3384.47 and 3413.70 cm^{-1} from 3376 cm^{-1}, respectively. These bands are assigned according to the literature.[21,22] The bands at 1051 and 1101 cm^{-1} are assigned to the $\nu_{as}(PO^{2-})$ end group and ν(P−O) of $NiPIm_2$, respectively. Similar bands are also observed for $NiPIm_{1.5}$. The IR spectra are displayed in Figure S1.

The IR spectrum of degraded PE with $NiPIm_2$ is displayed in Figure 1a. The band at 1687.89 cm^{-1} is due to the formation of ketone. Ketone is formed due to the decomposition of hydroperoxides by thermal oxidation.[23] The band at 1744.21 cm^{-1} is assigned to the carbonyl ester group.[24] This ester formation through oxidation under abiotic conditions is found similar to biotic oxidation as described by Schlegel.[25] The band at 1211.63 cm^{-1} is assigned to the ν(C−N) group of imidazole in the mixture and the C−H ring in-plane bending. This peak is shifted from 1180 cm^{-1} of $NiPIm_2$. The ring bend of imidazole of $NiPIm_2$ is shifted from ∼900 to 985.06 cm^{-1}. The ring stretch C═N is shifted downward to 1529.65 cm^{-1} from 1586 cm^{-1}. The amorphous C−C stretching frequency is absent at 1080 cm^{-1}.[26] The C−H bend is shifted from 1051 to 1025.60 cm^{-1}. The stretching frequency of N−H and its bend is absent at 3413 and 1433.99 cm^{-1}, respectively. This indicates the incorporation of PE with protonic imidazole. The −OH stretching frequency of water is observed at 3500−3800 cm^{-1}. This indicates that the degraded PE has the capacity to retain water molecules. The CH_2 asymmetric stretching is shifted from 2850 to 2865.89 cm^{-1}, while the symmetric stretching is shifted from 2785 to 2764.01 cm^{-1}.

The IR spectrum of degraded PVC with $NiPIm_2$ is displayed in Figure 1b. The band at 1686 cm^{-1}, which is found as a shoulder of the band at 1743.63 cm^{-1}, is assigned to the ketone group instead of the band at 1722 cm^{-1} for aliphatic ketone.[27,28] The carbonyl ester band is assigned at 1743.63 cm^{-1}. This ester formation for PVC is similar to that for PE. The bands at 1528.87, 1222, ∼1025 (shoulder), and 995 cm^{-1} are found similar to PE. The band at ∼3500 cm^{-1} is assigned to the O−H stretching frequency of water.

The IR spectrum of degraded PS with $NiPIm_2$ is displayed in Figure 1c. The band at 1759.32 cm^{-1} is assigned to the carbonyl ester group. The formation of ester can be attributed to the same mechanism as PE and PVC. The ketone functional group is also formed like PE and PVC. This is assigned at 1680.23 cm^{-1}. The band at 1595.66 cm^{-1} is assigned to the in-plane C═C bond of the aromatic ring instead of 1606 cm^{-1} assigned by You.[21] The stretching frequency of N−H is absent, and its bend is shifted from 1433 to 1404.60 cm^{-1}. This indicates the incorporation of polystyrene with protonic imidazole. The stretching frequency of P═O is shifted from 1329 to 1344 cm^{-1}. This is due to the participation of the PO_4^{3-} moiety in the thermal oxidation process. The band at 1051.48 cm^{-1} is assigned for the C−H bending in plane.[29] The ring bend of imidazole is assigned at 905.07 cm^{-1}. The asymmetric stretching of (P−O−P) bridge is assigned at 835.48 cm^{-1}. The N−H bend out of plane in imidazole is assigned at 630.29 cm^{-1}. The C−H bend out of plane and its stretching frequency in imidazole are assigned at 769.40 and 3156.07 cm^{-1}, respectively. The bands of phosphate and imidazole are assigned according to the published litera-

https://doi.org/10.1021/acsomega.1c04358
ACS Omega 2021, 6, 29869−29881

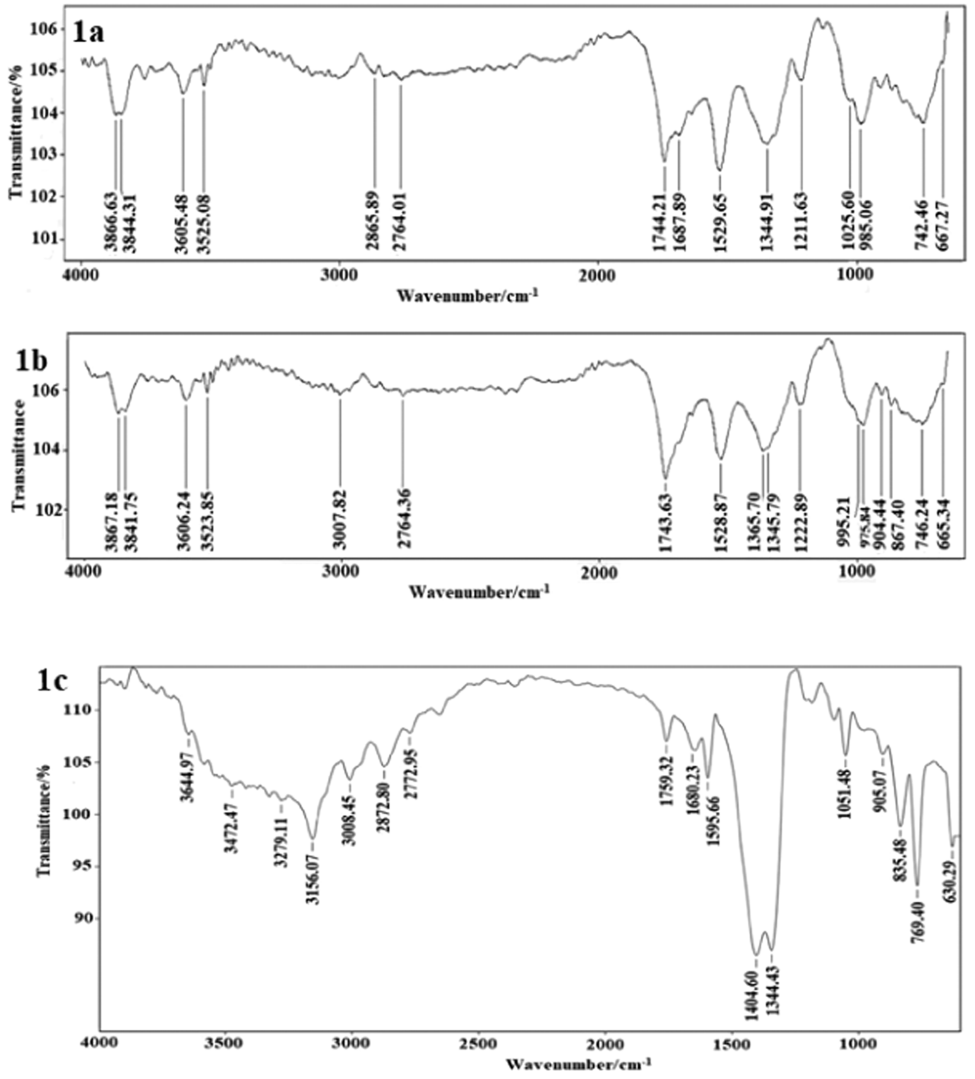

Figure 1. IR spectra of degraded residues. (a) IR spectrum of degraded residue of PE and $NiPIm_2$; (b) IR spectrum of degraded residue of PVC and $NiPIm_2$; and (c) IR spectrum of degraded residue of PS and $NiPIm_2$.

Table 2. Elemental Analysis of Nickel Nanocomposites

composite↓	experimental (%)					theoretical (%)				
elements→	Ni	P	C	N	H	Ni	P	C	N	H
$[Ni(C_3H_4N_2)(H_2O)_5](HPO_4)(H_2O)\cdot 0.3(C_3H_4N_2)$	17.03	8.50	13.01	10.02	5.65	16.72	8.83	13.33	10.36	5.18
$[Ni(C_3H_4N_2)(H_2O)_5](HPO_4)(H_2O)\cdot 0.4(C_3H_4N_2)\cdot H_2O$	16.04	7.98	13.42	10.53	5.57	15.60	8.25	13.40	10.42	5.48

ture.[30,31] The aromatic stretching frequency is assigned at 3008.45 cm^{-1} instead of 3025 cm^{-1} by Wu et al.[32]

2.2. Elemental Analysis. Elemental analysis of both the nickel composites was carried out using ICP-OES and C, H, N. The molecular weight and chemical formula of $NiPIm_{1.5}$ are 351.1 g mol^{-1} and $[Ni(C_3H_4N_2)(H_2O)_5](HPO_4)(H_2O)\cdot 0.3(C_3H_4N_2)$, while those of $NiPIm_2$ are 375.9 g mol^{-1} and $[Ni(C_3H_4N_2)(H_2O)_5](HPO_4)(H_2O)\cdot 0.4(C_3H_4N_2)\cdot H_2O$, respectively. The experimental and theoretical values of various proportions of elements, viz., Ni, P, C, N, and H, in terms of % are tabulated in Table 2.

2.3. X-ray Crystallography. The XRD pattern of $NiPIm_{1.5}$ is displayed in Figure 2a. This diffraction pattern confirmed the presence of imidazole in composite, which further conforms to the literature. Similarly, the conformity of the presence of imidazole in the diffraction pattern of $NiPIm_2$ is displayed in Figure 2b.[33] The XRD pattern of $NiPIm_2$ with PE, PVC, and PS is displayed in Figure 2c. This pattern is compared with polyester amide.[34] The mechanism of degradation of PE, PVC, and PS takes place through polyester. This is also further confirmed from the XRD pattern.

The crystallite size of $NiPIm_{1.5}$ and $NiPIm_2$ is calculated from the Debye–Scherrer formula. Using the peak broadening of the XRD profile, the calculated crystallite sizes are 32.6 and 31.6 nm for $NiPIm_{1.5}$ and $NiPIm_2$, respectively.

2.4. UV–Visible NIR Absorption Spectroscopy. The UV–vis–NIR spectra of $NiPIm_2$ and $NiPIm_{1.5}$ are displayed in Figure 3. The spectra of both composites execute a broad peak having λ_{max} = 410 nm. The calculated band gap (E_g) for both composites at 410 nm is 3.02 eV. This band gap is found similar to $(NH_4)_6[As_4Mo_6V_3O_{36}H_3]\cdot 5H_2O$.[35] This indicates that both composites are insulators. The refractive index (n) of

https://doi.org/10.1021/acsomega.1c04358
ACS Omega 2021, 6, 29869–29881

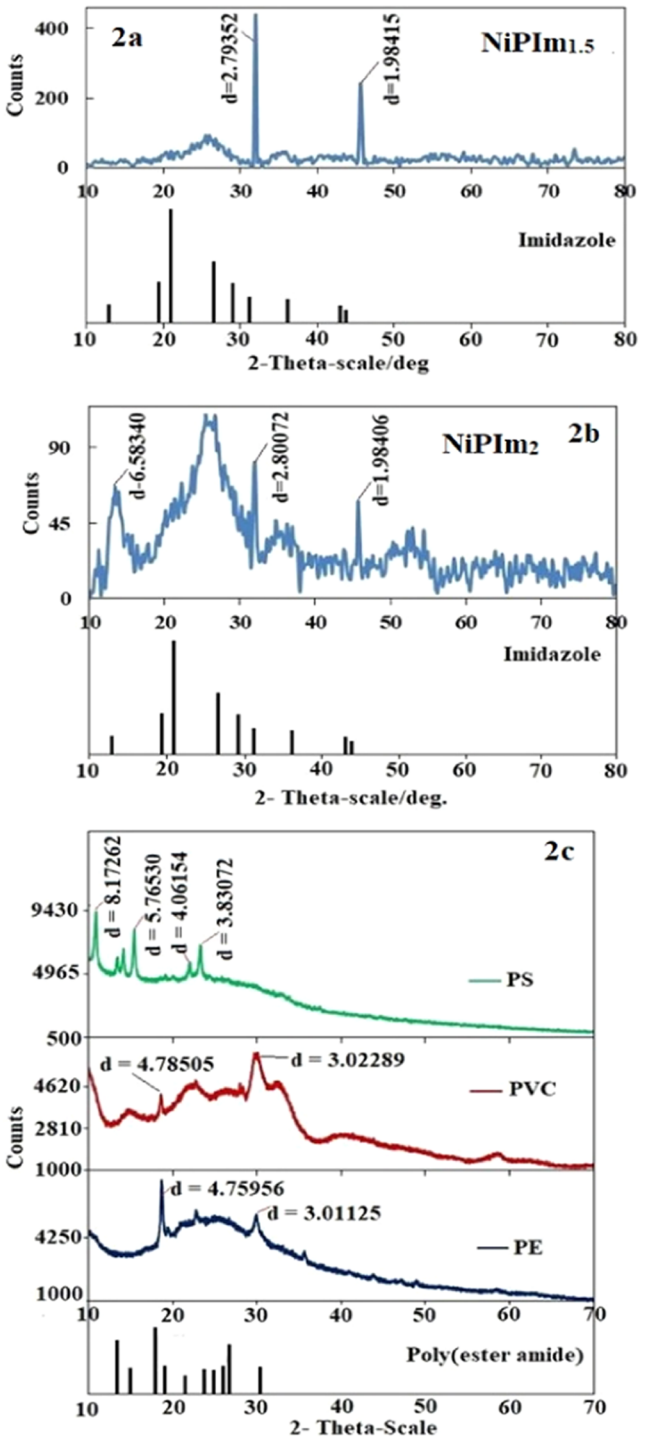

Figure 2. (a) XRD diffractogram of $NiPIm_{1.5}$; (b) XRD diffractogram of $NiPIm_2$; and (c) XRD diffractogram of degraded residue of $NiPIm_2$ and PE, PVC, and PS.

both composites is calculated using the Moss[36] and Ravindra[37] equation. The refractive index is found to be 2.36 and 2.21, respectively.

2.5. Thermal Analysis. *2.5.1. TG-DTA Analysis.* The decomposition steps of the thermogravimetric analysis of $NiPIm_{1.5}$ and $NiPIm_2$ are not clearly distinguished. The DTG curve of the $NiPIm_{1.5}$ indicates four decomposition processes up to 650 K. The peak temperatures are 363, 459.08, 542.76, and 591.92 K and the corresponding mass losses in % are 8.40,

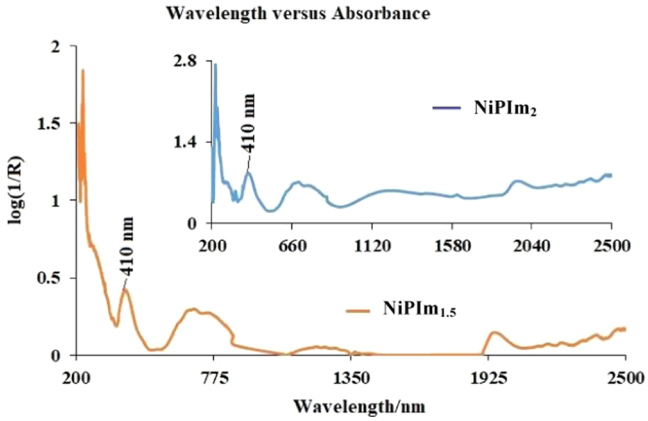

Figure 3. UV−vis−NIR spectrum of $NiPIm_{1.5}$ and $NiPIm_2$.

19.53, 28.76, and 39.42. All noncoordinated and coordinated water molecules along with 0.3 mole of imidazole are lost at 591.92 K. At this decomposition temperature, the % mass loss is 39.63 ± 0.21.

The DTG curve of $NiPIm_2$ indicates three decomposition processes and one shoulder at decomposition temperature peak 545.47 K up to 660 K. The three decomposition peak temperatures are 361.07, 461.95, and 545.47 K and a shoulder at 577.03 K is also found, whose corresponding mass losses in % are 8.21, 19.84, 31.19, and 40.04. All noncoordinated and coordinated water molecules along with 0.4 mole of imidazole are lost at 577.03 K. At this decomposition temperature, the % mass loss is 40.39 ± 0.35. The TG-DTG curves (301−1566 K) are displayed in Figure S2a. The DTA curves of $NiPIm_{1.5}$ and $NiPIm_2$ in the temperature range of 301−1566 K are displayed in Figure S2b. This curve indicates two endothermic peaks and one exothermic peak observed below 820 K. The two endothermic peaks of $NiPIm_{1.5}$ are at 376.62 K (sharp) and 555.58 K (broad), and one exothermic peak is sharp at 704.75 K. The enthalpy change (ΔH) at this exothermic peak is −853.26 J g^{-1}, while the enthalpy changes at the two endothermic peaks at 376.62 and 555.58 K are 888.39 and 1537.25 J g^{-1}, respectively.

All of the three peaks of $NiPIm_2$ are sharp. The two endothermic peaks and one exothermic peak are at 375.87, 558.67, and 699.50 K, respectively. The enthalpy change (ΔH) at the exothermic peak is −437.66 J g^{-1} at 699.50 K, while the enthalpy changes (ΔH) at 375.87 and 558.67 K are 888.26 and 1869.25 J g^{-1}, respectively.

The decomposition temperature is not clearly distinguished from the thermogravimetric analysis of PE, PVC, and PS composite materials. However, the decomposition temperatures of the above composite materials are clearly distinguished from the DTA curves. The TG-DTA curve of PE and $NiPIm_{1.5}$ composite material is displayed in Figure 4a. The endothermic and exothermic peaks of this composite material are at 353.98 and 462.50 K, respectively. This composite material decomposed at 462.50 K, which is completely different from the decomposition temperature of PE at 742.86 K and that of $NiPIm_{1.5}$ at 704.75 K. This composite material is formed by heating $NiPIm_{1.5}$ and PE at 353.98 K, which is much below the decomposition temperature of 462.50 K. Similarly, the TG-DTA curve of PE and $NiPIm_2$ composite material is displayed in Figure 4b. The DTA curve of this composite material indicates one endothermic and two exothermic peaks. The temperature of

https://doi.org/10.1021/acsomega.1c04358
ACS Omega 2021, 6, 29869−29881

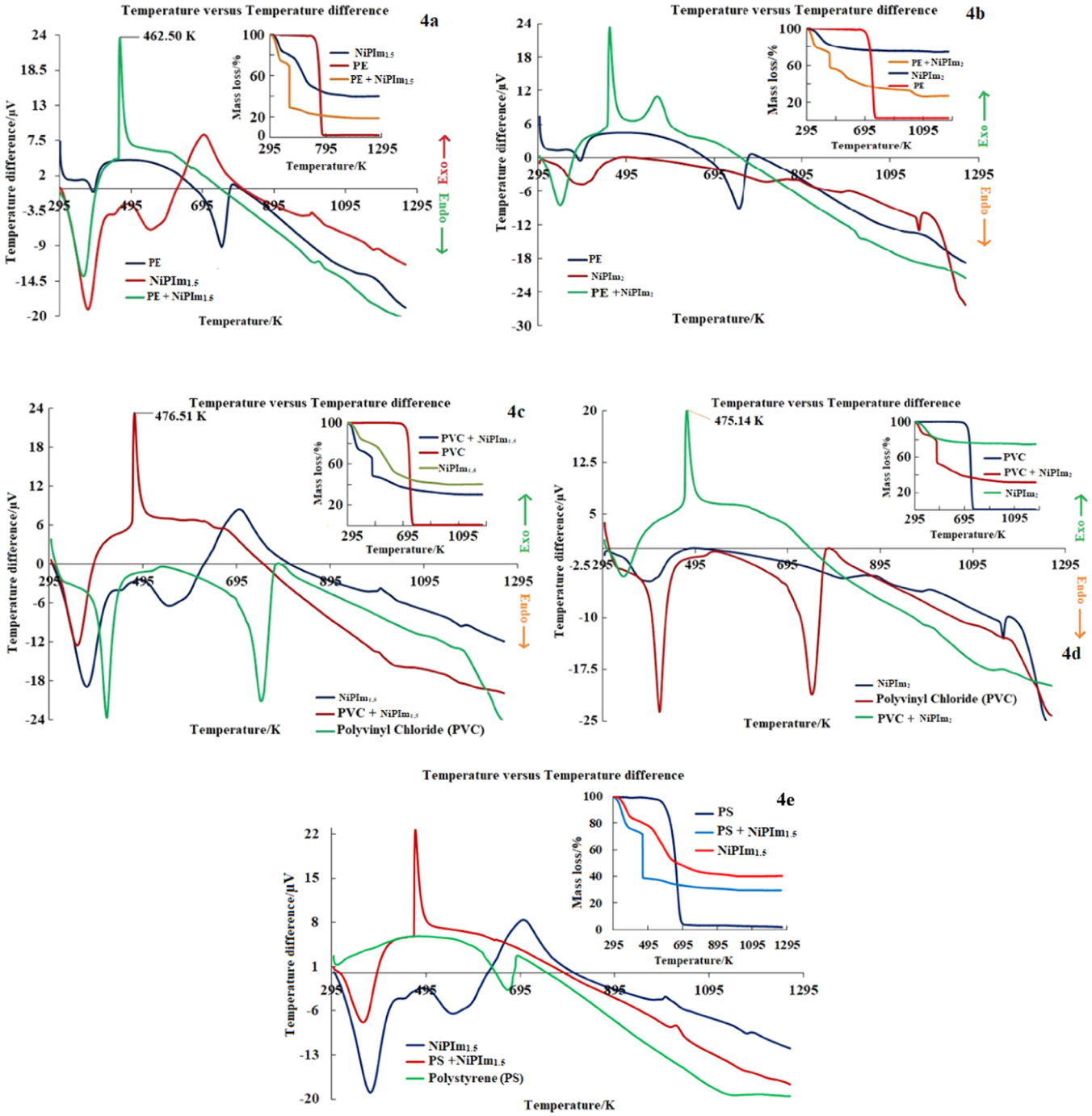

Figure 4. (a) Comparative TG-DTA curve of PE, $NiPIm_{1.5}$, and PE + $NiPIm_{1.5}$. (b) Comparative TG-DTA curve of PE, $NiPIm_2$, and PE + $NiPIm_2$. (c) Comparative TG-DTA curve of PVC, $NiPIm_{1.5}$, and PVC + $NiPIm_{1.5}$. (d) Comparative TG-DTA curve of PVC, $NiPIm_2$, and PVC + $NiPIm_2$. (e) Comparative TG-DTA curve of PS, $NiPIm_{1.5}$, and PS + $NiPIm_{1.5}$.

the endothermic peak is 338.76 K, and those of two exothermic peaks are 456.31 and 557.52 K. This composite material is decomposed at 456.31 K, and this temperature is much higher than the formation of composite material at 338.76 K. This indicates that the formation temperatures of both PE composite materials using $NiPIm_{1.5}$ and $NiPIm_2$ are much below the decomposition temperature.

The TG-DTA curve of PVC and the $NiPIm_{1.5}$ composite material is displayed in Figure 4c. The DTA curve of this composite material indicates one endothermic and one exothermic peak. The endothermic temperatures of PVC are 416.49 and 744.55 K. PVC with $NiPIm_{1.5}$ showed two peaks (one endo and one exo); the temperature of the endothermic peak is 349.27 K, while that of the exothermic peak is 476.51 K. Therefore, the formation temperature of composite material, 349.27 K, is much below the decomposition temperature, 476.51 K. Similarly, the TG-DTA of PVC and $NiPIm_2$ is displayed in Figure 4d. The DTA curve of this composite material indicates one endothermic and one exothermic peak. The temperatures of endothermic and exothermic peaks are 331.78 and 475.14 K, respectively. The temperature of formation of composite material is much below

https://doi.org/10.1021/acsomega.1c04358
ACS Omega 2021, 6, 29869−29881

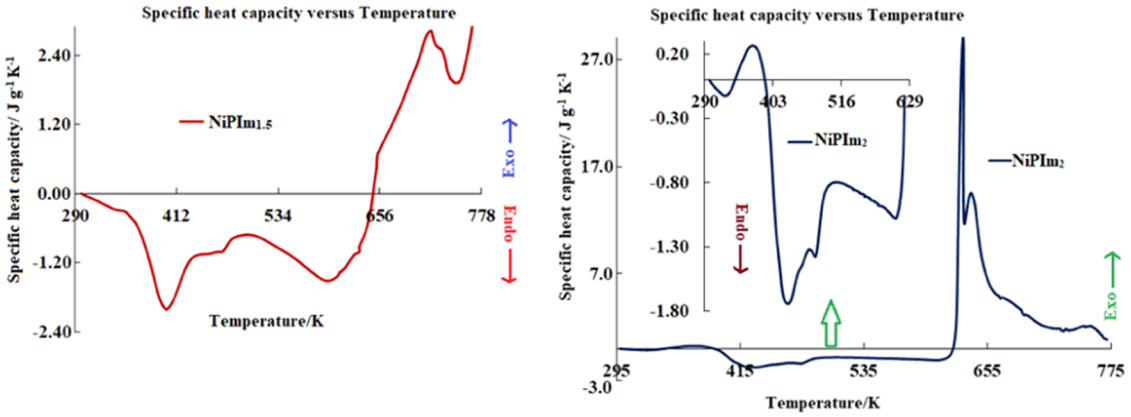

Figure 5. (a) DSC curve of $NiPIm_{1.5}$. (b) DSC curve of $NiPIm_2$ (lower temperature is incubated).

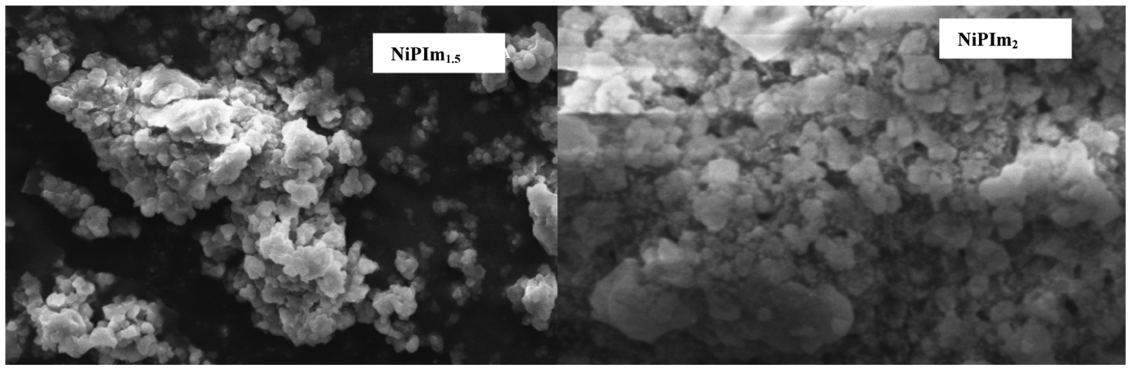

Figure 6. SEM images of $NiPIm_{1.5}$ and $NiPIm_2$.

the decomposition temperature. This indicates that the formation temperature of both PVC composite materials using $NiPIm_{1.5}$ and $NiPIm_2$ is much below the decomposition temperature.

The TG-DTA curve of polystyrene (PS) and $NiPIm_{1.5}$ composite material is displayed in Figure 4e. The DTA curve of this composite material indicates one endothermic peak and one exothermic peak. The temperatures of the endothermic and exothermic peaks of the PS composite material are 354.30 and 471.61 K, respectively. PS has one broad exothermic peak followed by one endothermic peak at temperature 659.21 K. The formation of the PS composite material at 354.30 K is much below the decomposition temperature at 471.61 K. All of the composite materials of PE, PVC, and PS are soluble in conc. HNO_3. Hence, this methodology of solubility in conc. HNO_3 can reduce the pollution level caused by PE, PVC, and PS.

2.5.2. Differential Scanning Calorimetry. The specific heat capacity versus temperature graph is plotted for $NiPIm_{1.5}$ and $NiPIm_2$ in the temperature range of 298−771 K (Figure 5a,b). The graph of $NiPIm_{1.5}$ shows three broad endothermic peaks and one exothermic peak (Figure 5a).

The temperatures of these four peaks are 396.66, 463.02, 596.53, and 713.54 K (exothermic). The negative specific heat capacity up to 646.19 K from 298 K is due to mass loss. The exothermic behavior of this material starts from 646.21 to 773.26 K, and the total specific heat capacity in this temperature range is −3300 J kg^{-1} K^{-1}. Similarly, the plot of $NiPIm_2$ shows four exothermic peaks and four endothermic peaks in the above temperature range (Figure 5b). The temperatures of these four endothermic peaks are 330.12, 429.44, 463.02, and 596.53 K. The temperatures of four exothermic peaks are 380.27, 630.64 (sharp), 636.97, and 749.79 K. The total specific heat capacity in the temperature range of 621.43−771 K is −850 J kg^{-1} K^{-1}. The negative specific heat capacity in both composites is due to mass loss. This is explained in terms of damping ratio (ζ). The anomalous negative specific heat in both composites is due to damping ratio (ζ) ≤ -1, while the positive specific heat capacity is due to the damping ratio (ζ) ≥ 1. The negative damping ratio indicates that the material is unstable with the increase in temperature. This instability is due to mass loss. The same is also confirmed by TG analysis.

2.6. SEM Analysis. SEM images of both composites are exemplified in Figure 6. The image of $NiPIm_{1.5}$ looks like a bunch of cotton flower at the resolution 50.0 kx, while the image of $NiPIm_2$ having a resolution of 10.0 kx looks like a bud of cotton flower.

2.7. Particle Size Analysis. The particle analysis of both the composites was carried out by high-resolution TEM. The average particle sizes of $NiPIm_{1.5}$ and $NiPIm_2$ are found to be 3.07 ± 0.84 and 8.08 ± 2.37 nm, respectively. As a result, it is confirmed that both the composites can be considered as nanomaterials. The polydispersity index (PDI) of the composites is determined to be 0.07 and 0.08. Hence, both the composites consist of monodisperse particles. The TEM images and histograms are shown in Figure 7.

2.8. Thermal Treatment. Nonbiodegradable polymers such as PE, PS, and PVC are thermally charged with $NiPIm_{1.5}$ and $NiPIm_2$ separately at 353 K for 120 min. All of the title polymers and composites were weighed before and after thermal charging. The collected results are tabulated in Table

https://doi.org/10.1021/acsomega.1c04358
ACS Omega 2021, 6, 29869−29881

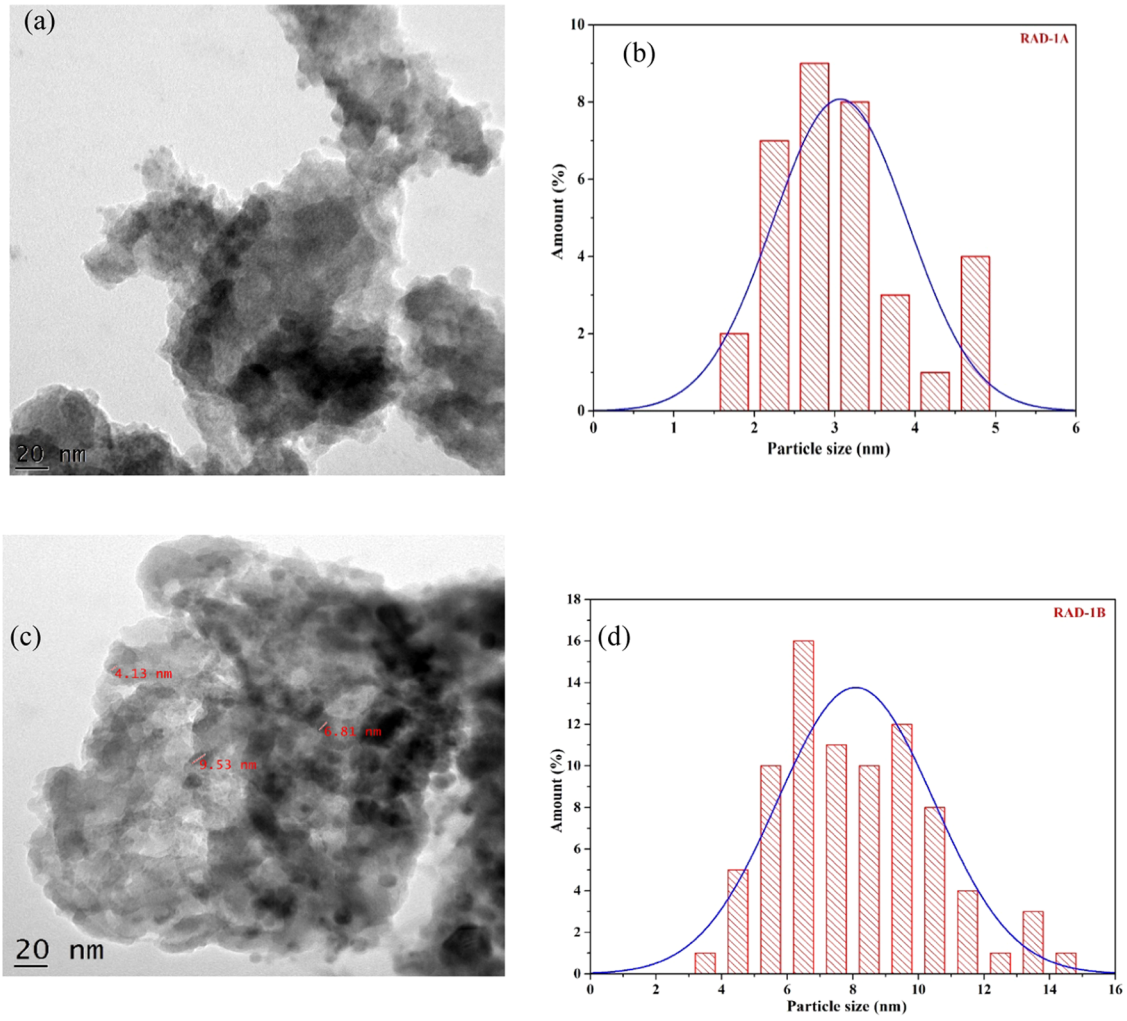

Figure 7. (a, b) TEM image and particle distribution histogram of $NiPIm_{1.5}$, respectively. (c, d) TEM image and particle distribution histogram of $NiPIm_2$, respectively.

Table 3. % of Thermally Degraded Residue of PE, PVC, and PS

				PE with sample (g)			
sl. no.	sample	sample (g)	PE without sample (g)	initial	final	weight loss (g)	weight loss (%)
1.	$NiPIm_{1.5}$	0.5484	1.0529	1.6013	1.4842	0.1171	7.3128
2.	$NiPIm_2$	0.5369	1.0826	1.6195	1.4065	0.213	13.1522
3.	without composite		1.0407	1.0407	1.0296	0.0111	1.0665
				PS with sample (g)			
			PS without sample (g)	initial	final		
4.	$NiPIm_{1.5}$	0.5163	0.8347	1.351	1.1891	0.1619	11.9837
5.	$NiPIm_2$	0.5024	0.9805	1.4829	1.2810	0.2019	13.6152
6.	without composite		0.8817	0.8817	0.8693	0.0124	1.4063
				PVC with sample (g)			
			PVC without sample (g)	initial	final		
7.	$NiPIm_{1.5}$	0.5026	2.0368	2.5394	2.4147	0.1247	4.9106
8.	$NiPIm_2$	0.5030	2.0057	2.5087	2.307	0.2017	8.04
9.	without composite		2.0292	2.0292	2.0282	0.001	0.0492

3. The degradation of PVC is exemplified in Figure 8, and the degradation processes of PE and PS are given in Supporting Information Figures S3 and S4. From the results, it is found that $NiPIm_2$ degraded these polymers more effectively than $NiPIm_{1.5}$. $NiPIm_2$ contains a higher proportion of imidazole than $NiPIm_{1.5}$, which facilitates the free radical mechanism more effectively, which is described in Section 3.

3. DISCUSSION

3.1. Stoichiometry Calculation. $NiPIm_{1.5}$, $[Ni(C_3H_4N_2)(H_2O)_5](HPO_4)(H_2O)\cdot 0.3(C_3H_4N_2)$, was synthesized by

https://doi.org/10.1021/acsomega.1c04358
ACS Omega 2021, 6, 29869−29881

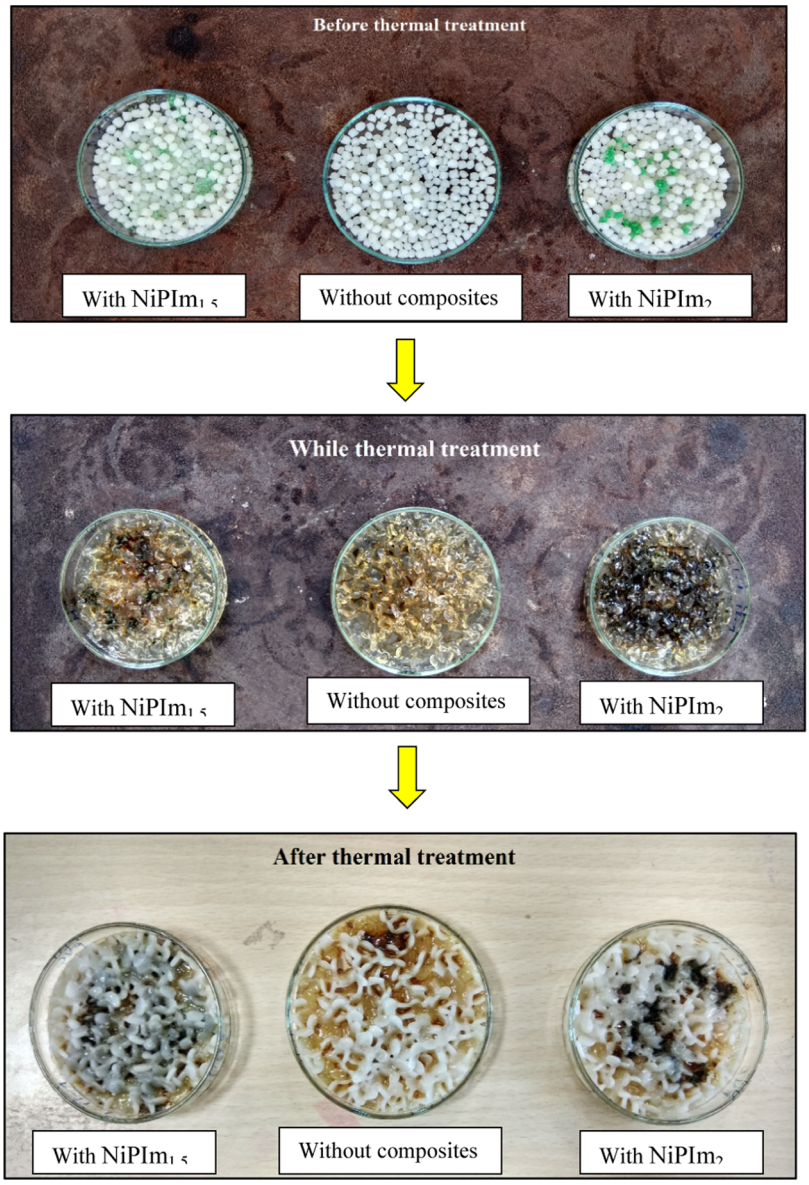

Figure 8. Thermo-oxidative degradation of PVC at 353 K for 120 min.

mixing nickel sulfate hexahydrate, phosphoric acid, and imidazole in a 1:1:1.5 ratio. The following reaction takes place during precipitation.

$$NiSO_4{\cdot}6H_2O + H_3PO_4 \rightarrow Ni(HPO_4) + 2H^+ + SO_4^{2-} + 6H_2O$$

$$Ni(HPO_4) + 2H^+ + SO_4^{2-} + 6H_2O + 1.5C_3H_4N_2 \rightarrow [Ni(C_3H_4N_2)(H_2O)_5]HPO_4(H_2O){\cdot}0.3C_3H_4N_2 + 2H^+ + SO_4^{2-} + 0.2C_3H_4N_2$$

The product of the reaction is further conformed from elemental analysis as well as TG-DTA measurement. The calculated and experimental weight loss for coordinated, noncoordinated, as well as 0.3 mole imidazole is found to be well coinciding with each other. Repeated washing of the above mixture eluted 0.2 mole of imidazole along with H_2SO_4.

Similarly, $NiPIm_2$, $[Ni(C_3H_4N_2)(H_2O)_5](HPO_4)(H_2O){\cdot}0.4(C_3H_4N_2){\cdot}H_2O$, was synthesized using $NiSO_4{\cdot}6H_2O$, H_3PO_4, and imidazole in a 1:1:2 ratio. The following reaction takes place during precipitation.

$$NiSO_4{\cdot}6H_2O + H_3PO_4 \rightarrow Ni(HPO_4) + 2H^+ + SO_4^{2-} + 6H_2O$$

$$Ni(HPO_4) + 2H^+ + SO_4^{2-} + 6H_2O + 2.0C_3H_4N_2 \rightarrow [Ni(C_3H_4N_2)(H_2O)_5]HPO_4(H_2O){\cdot}0.4C_3H_4N_2{\cdot}H_2O + 2H^+ + SO_4^{2-} + 0.6C_3H_4N_2$$

This product of the reaction is further conformed from elemental analysis as well as TG-DTA measurement. The calculated and experimental weight loss for coordinated, noncoordinated, as well as 0.4 mole of imidazole is found to be well coinciding with each other. Repeated washing of the above mixture with distilled water followed by ethanol eluted 0.6 mole imidazole along with H_2SO_4.

3.2. Mechanism of Thermo-oxidative Degradation.

From the IR analyses, it is evident that the formation of the

https://doi.org/10.1021/acsomega.1c04358
ACS Omega 2021, 6, 29869−29881

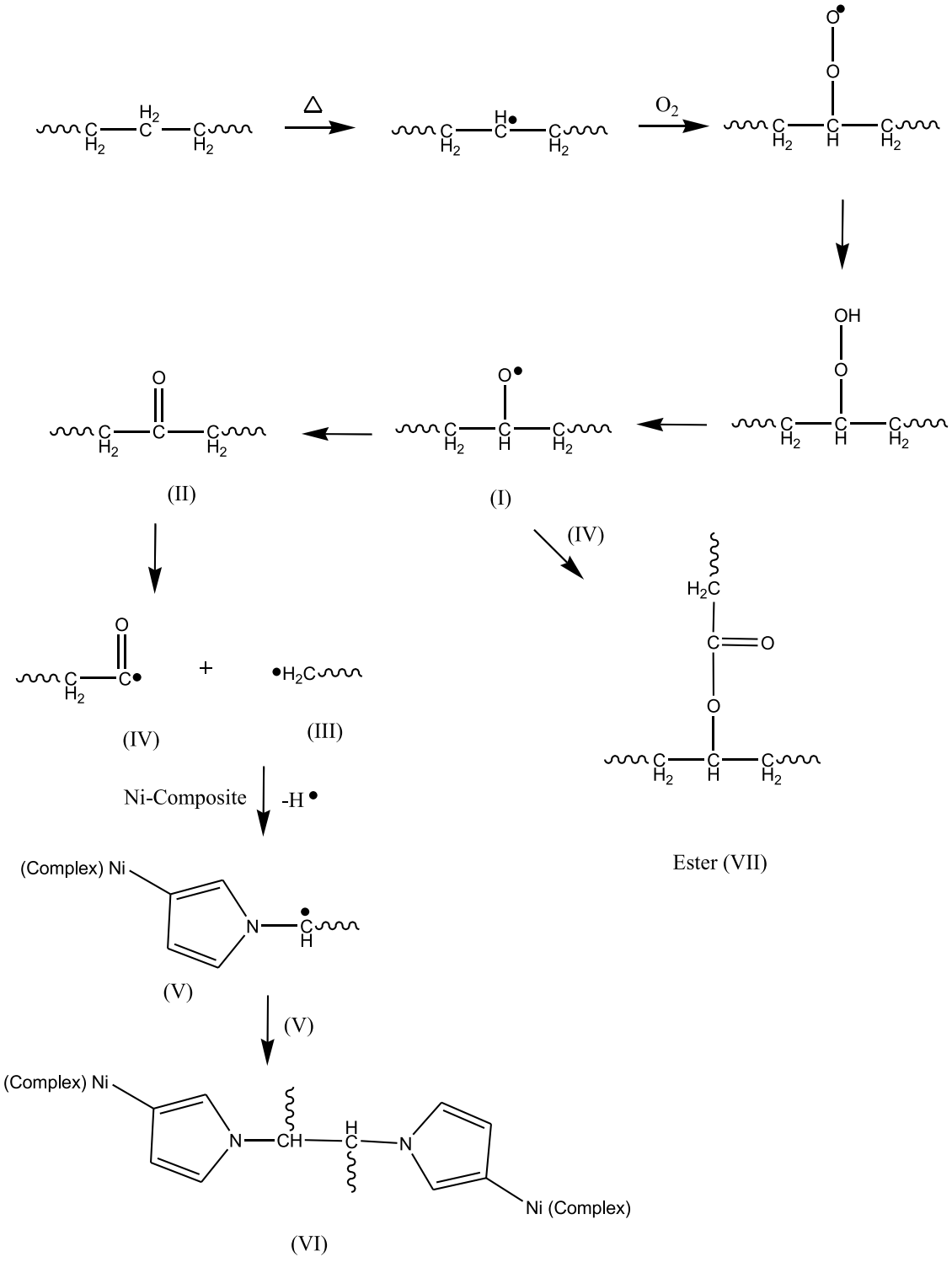

Figure 9. Thermo-oxidative mechanism of degradation of PE.

ketone group is facilitated easily due to the presence of the HPO_4 group in both composites. Hence, the nonbiodegradable PS, PE, and PVC degraded products contain a ketone group with both composites. The stretching frequencies at 1329 cm^{-1} (P═O) and 1101 cm^{-1} {$\nu_s(PO_3^{2-})$ end group} are absent in PS, PE, and PVC infrared spectra, which are found in $NiPIm_{1.5}$ and $NiPIm_2$. The C−N stretching frequency of free imidazole is shifted from ∼1320 cm^{-1} ($NiPIm_{1.5}$ and $NiPIm_2$) to ∼1344 cm^{-1} (broad).[38] This indicates that it forms a bond with PS, PVC, and PE free radicals. Thermal degradation of the polymers taking place by free radical mechanism with consequent formation of the corresponding ester is displayed in Figures 9−11.

The free radical (III) of degraded polymers combines with nonprotonated nitrogen of imidazole to form another free radical containing protonated imidazole. The protonated hydrogen sticks in imidazole are attached to nickel. This protonated hydrogen is believed to combine with free radical

https://doi.org/10.1021/acsomega.1c04358
ACS Omega 2021, 6, 29869−29881

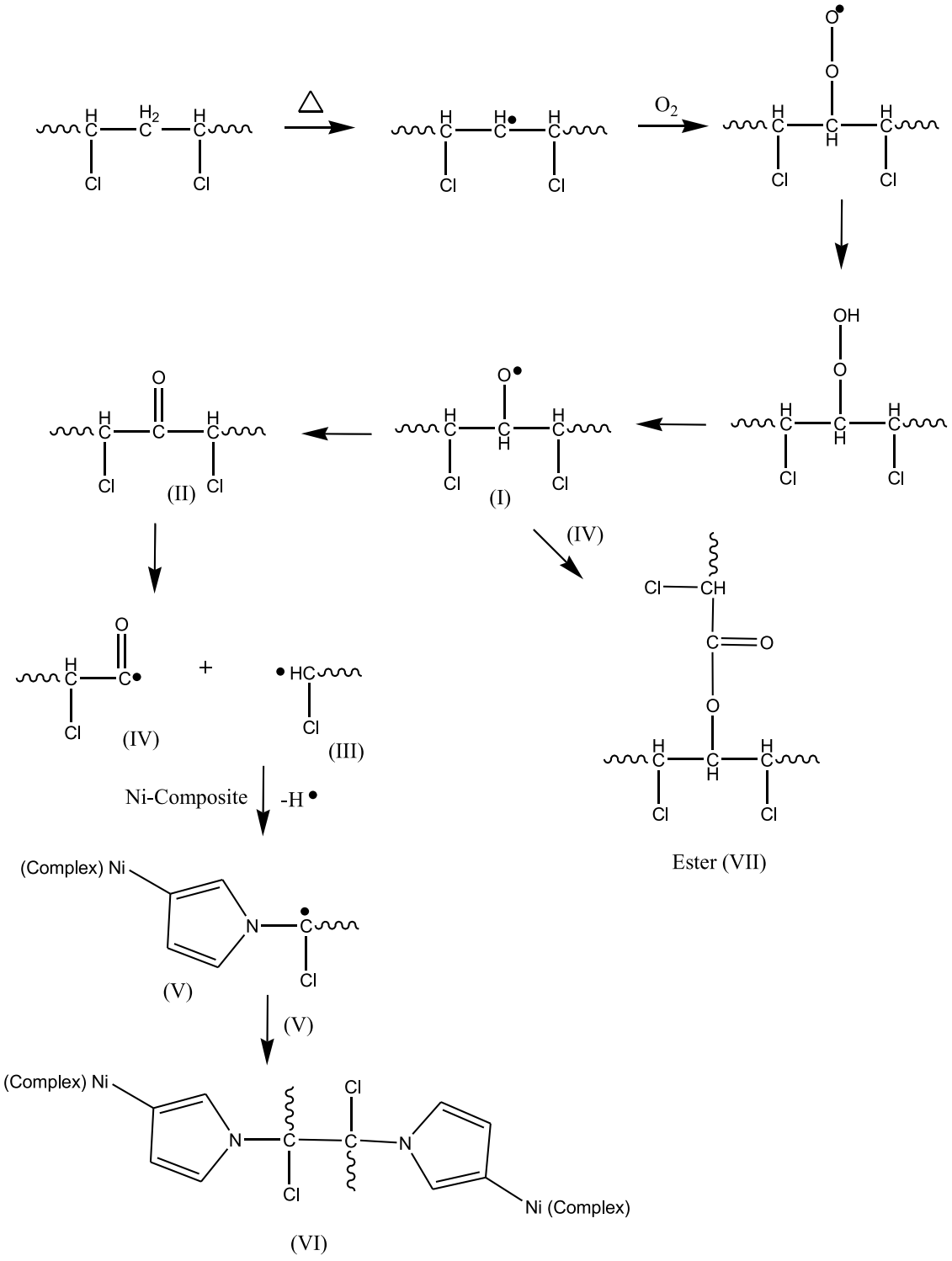

Figure 10. Thermo-oxidative degradation mechanism of PVC.

(III) with a loss of free radical H· and forms product (V). The product (I) combines with compound (IV) to form an ester (VII). The free radical compound (V) dimerizes to form compound (VI). The degradation mechanism of PE (Figure 9), PVC (Figure 10), and PS (Figure 11) is proposed according to the literature.[39−41]

In the case of PS degradation (Figure 11), the oxidation results are compound (I) and carboxyl compound (II). The compounds (III) and (IV) form from (II) then (III) combine with the nitrogen of the imidazole ring present in the composite with a simultaneous loss of hydrogen radical and forms (V). Similar to the mechanism shown in the case of PE, (IV) combines with (I), leading to the ester (VI) formation, and the product (VII) is formed by the dimerization of (V).

The higher degradation rates of polymers with $NiPIm_{1.5}$ and $NiPIm_2$ are explained with the help of DSC analysis. Up to 340.49 K, $NiPIm_2$ exhibited endothermic nature, and then it exhibited exothermic nature up to 389.67 K, which means that

https://doi.org/10.1021/acsomega.1c04358
ACS Omega 2021, 6, 29869−29881

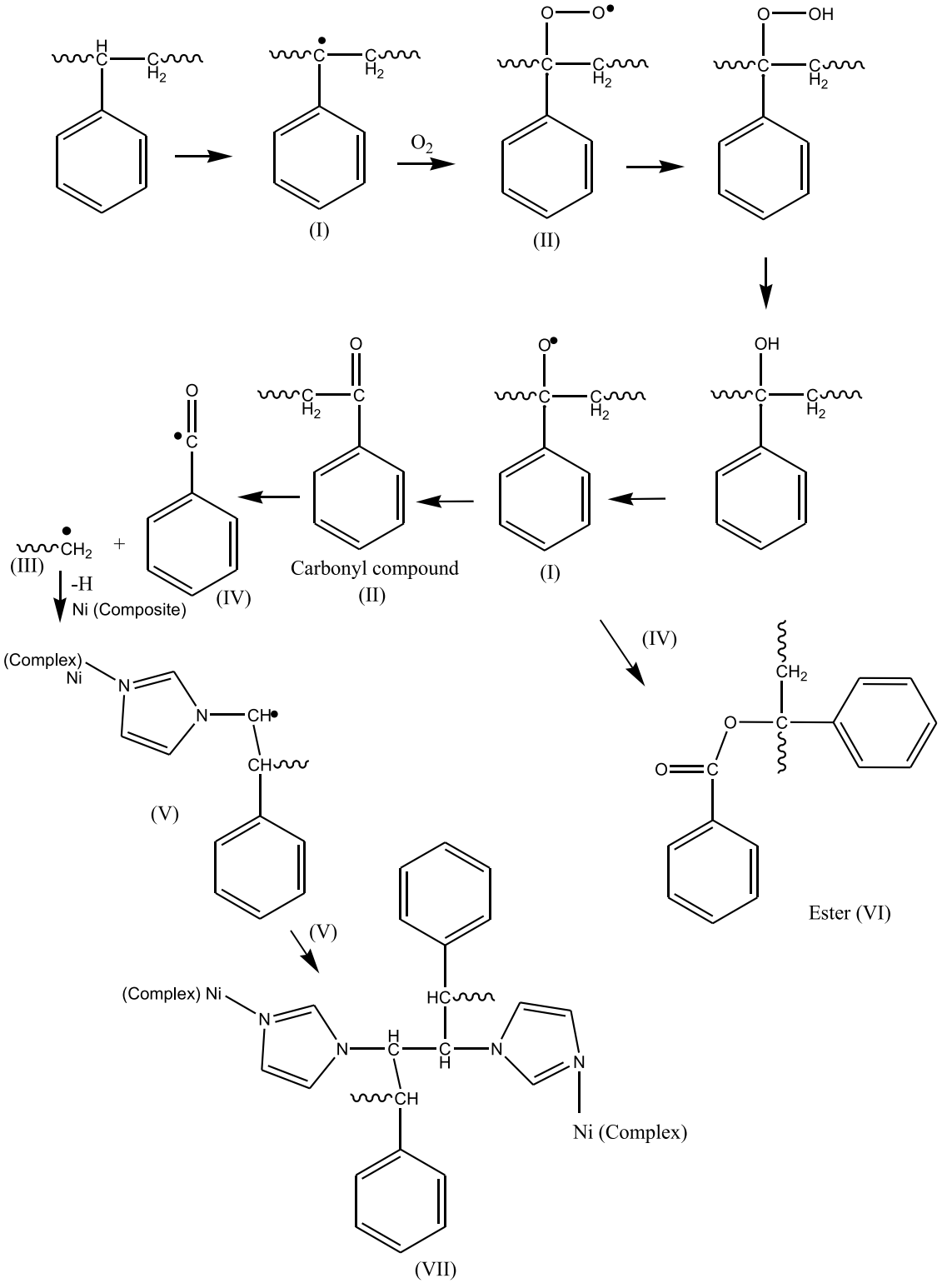

Figure 11. Thermo-oxidative degradation mechanism of PS.

it dissipated heat to polymer since the thermal treatment is carried out at 353 K; ultimately, the degradation process accelerated in its presence. Moreover, the specific heat capacities of $NiPIm_2$ and $NiPIm_{1.5}$ are −348.64 and −148.42 J kg^{-1} K^{-1}, respectively, at 353 K. As a result, $NiPIm_2$ transfers more amount of heat to the polymer than $NiPIm_{1.5}$.

3.3. Comparison. Li et al.[15] reported a 45.6% degradation of PE by the photocatalytic process and the time taken for the entire process is 240 h. Kumar et al.[14] reported a 96.6% degradation of PE, but at 823 K, we tried to decrease the time and heating temperature to 120 min and 353 K, respectively, and achieved a 13.15% degradation. A 41.1% weight loss of PVC at 523 K was reported by López et al.[16] Our experiment was carried out at 353 K and attained 8.04% PVC degradation with $NiPIm_2$. Similarly, in the case of PS, we also carried out the same experiment as for PE and PVC degradation and

https://doi.org/10.1021/acsomega.1c04358
ACS Omega 2021, 6, 29869−29881

attained a 13.61% degradation. One of the interests of our work is low-smoke degradation, which may lead to easy recyclization of polymers.

4. CONCLUSIONS

Two imidazole-based nickel nanocomposites were synthesized under ambient condition. Both are characterized using various analytical techniques such as IR, elemental analysis (ICP-OES and C, H, N), XRD, TG-DTA, UV−vis−NIR, FESEM, and HRTEM. Both the composites were used in the thermo-oxidative degradation of PE, PVC, and PS, and these degradation processes are conducted at 353 K for 120 min. The % degradation values of polymers in the presence of $NiPIm_{1.5}$ and $NiPIm_2$ are PE—13.1522%, PS—13.6152, and PVC—8.04, and PE—7.3128, PS—11.9837, and PVC—4.9106, respectively. $NiPIm_2$, $[Ni(C_3H_4N_2)(H_2O)_5](HPO_4)\cdot(H_2O)\cdot 0.4(C_3H_4N_2)\cdot H_2O$, degraded the title polymers more in proportion than $NiPIm_{1.5}$, $[Ni(C_3H_4N_2)(H_2O)_5](HPO_4)\cdot(H_2O)\cdot 0.3(C_3H_4N_2)$, due to its thermal property, and it is confirmed by the calorimetric study. The results indicate that the thermal degradation is due to the formation of polyester via the ketone group. The average particle sizes of the composites are determined to be 3.07 ± 0.84 and 8.08 ± 2.37 nm.

5. EXPERIMENTAL SECTION

5.1. Reagent and Synthesis of Nanocomposites. Nickel sulfate hexahydrate ($NiSO_4\cdot 6H_2O$) and orthophosphoric acid (H_3PO_4, 86%) were mixed in a 1:1 molar ratio by constant stirring for 48 h. The resulted homogeneous mixture was divided into two portions, and each portion is treated separately with 1.5 and 2 moles of imidazole. After addition of imidazole, each portion of the mixture was stirred for 48 h in a magnetic stirrer to ensure complete neutralization. Portion 1 neutralized with 1.5 moles of imidazole gives light greenish $NiPIm_{1.5}$, and portion-2 neutralized with 2.0 moles of imidazole gives deep greenish $NiPIm_2$. These colored residues were filtered, washed, and dried in ethanol. Both the composites were synthesized under ambient conditions. Analar-grade chemicals from Sigma-Aldrich were used for the synthesis of the composites.

5.2. Instrumentation. All analyses such as IR, DSC, TG-DTA, ICP-OES, FESEM, and XRD were carried out to characterize the above composites by adopting the same procedure as reported in our previous work.[17] The functional groups were identified from the FT-IR study using a Thermo Nicolet Nexus 670 setup between 400 and 4000 cm^{-1}. The specific heat capacity of both composites was measured at a heating rate of 10 K min^{-1} by a differential scanning calorimetry DSC Discovery 250 equipment. All DSC measurements were performed in an aluminum crucible at a normal atmosphere in the temperature range of 298−771 K. Thermal decomposition studies, thermogravimetric analysis (TGA), and derivative thermogravimetry (DTG), were done in the temperature range of 295−1295 K for composite materials of polymers with $NiPIm_{1.5}$ and $NiPIm_2$, while for original composites, experiments were done at 301−1566 K on a TAQ600 thermal analyzer in normal atmosphere using the aluminum crucible. For ICP-OES analysis, both were dissolved in 10 mL of HNO_3 at 30% (v/v) and the volume was made up to 100 mL using high-performance liquid chromatography (HPLC)-grade water for elemental analysis. X-ray diffraction (XRD) analysis was carried out on a PANalytical Empyrean XRD with copper Kα radiation (λ = 1.5406 Å), 2θ range of 10−80°, a step of 0.01°, and an acquisition time of 1 s for each step. The crystallite size was determined from the FWHM of XRD. Both nanocomposites were used to decompose the above-said materials thermally at 333 K. The decomposed residue was dissolved in concentrated HNO_3 and sufficiently diluted with distilled water. The solution was dried in a silica gel desiccator. The dried residue was used for IR and XRD analyses.

■ ASSOCIATED CONTENT

Supporting Information

The Supporting Information is available free of charge at https://pubs.acs.org/doi/10.1021/acsomega.1c04358.

IR spectra of nanocomposites; TG, DTG, and DTA thermograms; thermo-oxidative degradation processes of PE and PS; and degradation methods of PE, PVC, and PS (PDF)

■ AUTHOR INFORMATION

Corresponding Author

Rudrarapu Aravind − *Department of Chemistry, IcfaiTech (Faculty of Science and Technology), IFHE, Hyderabad, Telangana 501203, India;* orcid.org/0000-0001-7770-6077; Email: aravind.r@ifheindia.org, aravindrudrarapu@gmail.com

Authors

Akash Kumar Sahu − *Department of Chemistry, IcfaiTech (Faculty of Science and Technology), IFHE, Hyderabad, Telangana 501203, India*

Gouri Sankhar Brahma − *Department of Chemistry, IcfaiTech (Faculty of Science and Technology), IFHE, Hyderabad, Telangana 501203, India*

Trilochan Swain − *P.G. Department of Chemistry, Fakir Mohan University, Balasore, Odisha 756089, India*

Complete contact information is available at: https://pubs.acs.org/10.1021/acsomega.1c04358

Author Contributions

All of the authors have given approval to the final version of the manuscript.

Funding

This work was supported by the Department of Chemistry, IcfaiTech (Faculty of Science & Technology), The ICFAI Foundation for Higher Education, Hyderabad.

Notes

The authors declare no competing financial interest.

■ ACKNOWLEDGMENTS

The corresponding author, R.A., is thankful to the Department of Chemistry, IcfaiTech (FST), The ICFAI Foundation for Higher Education, Hyderabad, for necessary financial support. A.K.S. and G.S.B. are also grateful to the IFHE Hyderabad. T.S. is grateful to the F.M. University for granting permission to become associated with this work.

■ REFERENCES

(1) Chiellini, E.; Corti, A.; D'Antone, S.; Baciu, R. Oxo-Biodegradable Carbon Backbone Polymers - Oxidative Degradation of Polyethylene under Accelerated Test Conditions. *Polym. Degrad. Stab.* **2006**, *91*, 2739−2747.

(2) David, C. Chapter 1 Thermal Degradation of Polymers. *Compr. Chem. Kinet.* **1975**, *14*, 1−173.
(3) Holmström, A.; Andersson, A.; Sörvik, E. M. Thermo-Oxidative Degradation of Polyethylene-III. The Effect of Titanium Dioxide Pigments on Low-Density Polyethylene. *Eur. Polym. J.* **1977**, *13*, 483−487.
(4) Hrdlovic, P.; Pavlinec, J.; Jellinek, H. H. G. Degradation of Polymers and Morphology. Photo- Oxidative Degradation of Isotactic Polystyrene in Presence of Sulfur Dioxide as Function of Polymer Crystallinity. *J. Polym. Sci., Part A-1: Polym. Chem.* **1971**, *9*, 1235−1245.
(5) Smith, R.; Oliver, C.; Williams, D. F. The Enzymatic Degradation of Polymers In Vitro. *J. Biomed. Mater. Res.* **1987**, *21*, 991−1003.
(6) Basedow, A. M.; Klaus Heinrich, E. Ultrasonic Degradation of Polymers in Solution. In *Physical Chemistry*; Springer, 1977; Vol. *22*, pp 83−148.
(7) Xiao-jing, L.; Guan-jun, Q.; Jie-rong, C. The Effect of Surface Modification by Nitrogen Plasma on Photocatalytic Degradation of Polyvinyl Chloride Films. *Appl. Surf. Sci.* **2008**, *254*, 6568−6574.
(8) Speight, J. G. Monomers, Polymers, and Plastics. In *Handbook of Industrial Hydrocarbon Processes*; Gulf Professional Publishing, 2020.
(9) Jen-hou, L. Zum Verhalten von Bakteriengemischen Gegenuber Polyathylen Verschiedenen Mittleren Molekulargewichts. *Kunststoffe* **1961**, *51*, 317−320.
(10) Nisar, J.; Khan, M. S.; Iqbal, M.; Shah, A.; Ali, G.; Sayed, M.; Khan, R. A.; Shah, F.; Mahmood, T. Thermal Decomposition Study of Polyvinyl Chloride in the Presence of Commercially Available Oxides Catalysts. *Adv. Polym. Technol.* **2018**, *37*, 2336−2343.
(11) Kaplan, D. L.; Hartenstein, R.; Sutter, J. Biodegradation of Polystyrene, Poly(Methyl Methacrylate), and Phenol Formaldehyde. *Appl. Environ. Microbiol.* **1979**, *38*, 551−553.
(12) Zhu, X. Thermal and Thermo-Oxidative Degradation of Polystyrene with Ammonium Polyphosphate. *J. Fire Sci.* **1996**, *14*, 443−464.
(13) Okada, M. Chemical Syntheses of Biodegradable Polymers. *Prog. Polym. Sci.* **2002**, *27*, 87−133.
(14) Kumar, S.; Singh, R. K. Thermolysis of High-Density Polyethylene to Petroleum Products. *J. Pet. Eng.* **2013**, *2013*, 1−7.
(15) Li, S.; Xu, S.; He, L.; Xu, F.; Wang, Y.; Zhang, L. Photocatalytic Degradation of Polyethylene Plastic with Polypyrrole/TiO2 Nanocomposite as Photocatalyst. *Polym.-Plast. Technol. Eng.* **2010**, *49*, 400−406.
(16) López, A.; De Marco, I.; Caballero, B. M.; Laresgoiti, M. F.; Adrados, A. Dechlorination of Fuels in Pyrolysis of PVC Containing Plastic Wastes. *Fuel Process. Technol.* **2011**, *92*, 253−260.
(17) Aravind, R.; Brahma, G. S.; Swain, T.; Sahu, A. K. Synthesis, Characterization of Imidazole-Based Copper Complex Mixtures and Study of Their Thermal Behaviour. *Int. J. Energy Res.* **2021**, 9179−9192.
(18) Mahdi, A. S.; Awad, A. A.; Hasson, M. M. Preparation and Study Mixed Complexes of Salicylaldehyde Copper (II) and Nickel (II) with Imidazole. *Acta Chim. Pharm. Indica* **2017**, *7*, 1−7.
(19) Rudrarapu, A.; Brahma, G. S.; Swain, T. Heat Repellent Behavior of Cobalt-Based Imidazole Containing Phosphate and Meta-Phosphate Complex Mixtures. *Int. J. Energy Res.* **2021**, *45*, 13911−13924.
(20) Thavamani, S. S.; Peter Amaladhas, T. Encapsulation of Cu(II), Ni(II) and V(IV) - Imidazole Complexes in Fly Ash Zeolite, Characterisation and Catalytic Activity towards Hydroxylation of Phenol. *J. Mater. Environ. Sci.* **2016**, *7*, 2314−2327.
(21) You, X.; Zhu, L. Synthesis, Crystal Structure and Characterization of an Organically Templated Cobalt Phosphate Supramolecule. *Ind. J. Chem. Sec-A* **2010**, *49*, 1478−1482.
(22) Ghoneim, N. A.; Abdelghany, A. M.; Abo-Naf, S. M.; Moustafa, F. A.; Elbadry, K. M. Spectroscopic Studies of Lithium Phosphate, Lead Phosphate and Zinc Phosphate Glasses Containing TiO2: Effect of Gamma Irradiation. *J. Mol. Struct.* **2013**, *1035*, 209−217.
(23) Carlsson, D. J.; Garton, A.; Wiles, D. M. Initiation of Polypropylene Photooxidation. 2. Potential Processes and Their Relevance to Stability. *Macromolecules* **1976**, *9*, 695−701.
(24) Albertsson, A. C.; Griffin, G. J. L.; Karlsson, S.; Nishimoto, K.; Watanabe, Y. Spectroscopic and Mechanical Changes in Irradiated Starch-Filled LDPE. *Polym. Degrad. Stab.* **1994**, *45*, 173−178.
(25) Schlegel, H.-G. *Allgemeine Mikrobiologie*, 8th ed.; Georg Thieme Verlag: New York, 2007.
(26) Krimm, S.; Liang, C. Y.; Sutherland, G. B. B. M. Infrared Spectra of High Polymers. II. Polyethylene. *J. Chem. Phys.* **1956**, *25*, 549−562.
(27) Ahmed, D. S.; El-Hiti, G. A.; Yousif, E.; Hameed, A. S. Polyphosphates as Inhibitors for Poly(Vinyl Chloride) Photodegradation. *Molecules* **2017**, *22*, No. 1849.
(28) Hadi, A. G.; Jawad, K.; El-Hiti, G. A.; Alotaibi, M. H.; Ahmed, A. A.; Ahmed, D. S.; Yousif, E. Photostabilization of Poly(Vinyl Chloride) by Organotin(IV) Compounds against Photodegradation. *Molecules* **2019**, *24*, No. 3557.
(29) León-Bermúdez, A. Y.; Salazar, R. Synthesis and Characterization of the Polystyrene - Asphaltene Graft Copolymer by FT-IR Spectroscopy. *CT&F, Cienc., Tecnol. Futuro* **2008**, *3*, 157−167.
(30) Velli, L. L.; Varsamis, C. P. E.; Kamitsos, E. I.; Möncke, D.; Ehrt, D. Structural Investigation of Metaphosphate Glasses. *Phys. Chem. Glasses* **2005**, *46*, 178−181.
(31) Ronalds Leon, M. *The Infrared Spectroscopic Comparison of Metal Complexes of Imidazole and Structurally Related Compounds*; Kansas State University, 1969.
(32) Wu, H. D.; Wu, S. C.; Wu, I. D.; Chang, F. C. Novel Determination of the Crystallinity of Syndiotactic Polystyrene Using FTIR Spectrum. *Polymer* **2001**, *42*, 4719−4725.
(33) Trivedi, M. K.; Dahryn Trivedi, A. B.; Gunin Saikia, G. N. Physical and Structural Characterization of Biofield Treated Imidazole Derivatives. *Nat. Prod. Chem. Res.* **2015**, *03*, No. 1000187.
(34) Khairou, K. S.; Abdullah, M. A.; Aly, K. I.; Nahas, N. M.; Al-Bonian, A. M. Synthesis and Characterization of New Poly(Ester-Amide)s Containing Diarylidenecyclohexanone in the Main Chain. Part: II. *Arabian J. Chem.* **2009**, *2*, 65−71.
(35) Gao, Q.; Xu, L. A New Mo/V-Arsenite-Based Heteropolyoxometalate [As 4 Mo 6 V 3 O 36 H 3] 6−: Synthesis, Crystal Structure and Surface Photovoltage. *Inorg. Chem. Commun.* **2019**, *105*, 125−128.
(36) Moss, T. S. Relations between the Refractive Index and Energy Gap of Semiconductors. *Phys. Status Solidi B* **1985**, *131*, 415−427.
(37) Ravindra, N. M.; Sushil, A.; Srivastava, V. K. On the Penn Gap in Semiconductors. *Phys. Status Solidi B* **1979**, *93*, K155−K160.
(38) Ramasamy, R. Vibrational Spectroscopic Studies of Imidazole. *Arm. J. Phys.* **2015**, *8*, 51−55.
(39) Kiatkamjornwong, S.; Sonsuk, M.; Wittayapichet, S.; Prasassarakich, P.; Vejjanukroh, P. C. Degradation of Styrene-g-Cassava Starch Filled Polystyrene Plastics. *Polym. Degrad. Stab.* **1999**, *66*, 323−335.
(40) Arutchelvi, J.; Sudhakar, M.; Arkatkar, A.; Doble, M.; Bhaduri, S.; Uppara, P. V. Biodegradation of Polyethylene and Polypropylene. *Indian J. Biotechnol.* **2008**, *7*, 9−22.
(41) Liu, J.; Lv, Y.; Luo, Z.; Wang, H.; Wei, Z. Molecular Chain Model Construction, Thermo-Stability, and Thermo-Oxidative Degradation Mechanism of Poly(Vinyl Chloride). *RSC Adv.* **2016**, *6*, 31898−31905.

https://doi.org/10.1021/acsomega.1c04358
ACS Omega 2021, 6, 29869−29881